Analyses of transient chaotic time series

Mukeshwar Dhamala,[1] Ying-Cheng Lai,[2,3] and Eric J. Kostelich[2]

[1]*School of Physics, Georgia Institute of Technology, Atlanta, Georgia 30332*
and School of Medicine, Emory University, Atlanta, Georgia 30322
[2]*Department of Mathematics, Arizona State University, Tempe, Arizona 85287*
[3]*Department of Electrical Engineering and Department of Physics, Center for Systems Science and Engineering Research,*
Arizona State University, Tempe, Arizona 85287

We address the calculation of correlation dimension, the estimation of Lyapunov exponents, and the detection of unstable periodic orbits, from transient chaotic time series. Theoretical arguments and numerical experiments show that the Grassberger-Procaccia algorithm can be used to estimate the dimension of an underlying chaotic saddle from an ensemble of chaotic transients. We also demonstrate that Lyapunov exponents can be estimated by computing the rates of separation of neighboring phase-space states constructed from each transient time series in an ensemble. Numerical experiments utilizing the statistics of recurrence times demonstrate that unstable periodic orbits of low periods can be extracted even when noise is present. In addition, we test the scaling law for the probability of finding periodic orbits. The scaling law implies that unstable periodic orbits of high period are unlikely to be detected from transient chaotic time series.

I. INTRODUCTION

In many experiments, the measured signals often exhibit irregular behavior during an initial interval before finally settling into an asymptotic state that is nonchaotic. The conventional wisdom may be simply to disregard the transient portion of the data and to concentrate on the final state. By doing this, however, information about the system may be lost, because the irregular part of the data may contain important hints about the system dynamics. This is particularly true when the underlying dynamics is deterministic and exhibits transient chaos [1–3]. While there has been a tremendous amount of work on analyzing time series from chaotic attractors [4], to our knowledge the problem of analyzing *transient* chaotic time series has not been addressed [5]. The purpose of this paper is to address some aspects of this important problem: computing the correlation dimension from experimentally measured transient chaotic time series, extracting Lyapunov exponents, and detecting unstable periodic orbits embedded in the underlying chaotic invariant set that is responsible for transient chaos.

Nonattracting chaotic saddles are the dynamical invariant sets that give rise to transient chaos [1–3]. Because such a saddle is chaotic but nonattracting, a trajectory starting from a typical initial condition in a phase-space region containing the saddle stays near the saddle for a time (exhibiting chaotic behavior), and then exits the region and asymptotes to a final state. Physically, chaotic saddles lead to observable phenomena such as chaotic scattering [6], fractal basin boundaries [7], fractal concentrations of passive particles advected in open hydrodynamical flows [8], and fractal distribution of chemicals in environmental flows [9]. Mathematically, chaotic saddles are closed, bounded, and invariant sets with dense orbits. Like chaotic attractors, a chaotic saddle has embedded within it an infinite number of unstable periodic orbits that constitute its ''skeleton'' [10].

The primary difficulty in dealing with a transient chaotic system is that the chaotic phases, which contain the essential information about the chaotic saddle, are relatively short. In this paper, we show that many of the standard algorithms that are used to estimate dynamical quantities from time series of sustained chaotic processes can be applied to ensembles of shorter, transient chaotic time series. It is not necessary to construct a single long time series from a set of shorter ones. All that is required is a collection of transient time series, starting from different initial conditions but for the same system parameters.

The organization of this paper is as follows. In Sec. II, we argue and provide numerical support that the Grassberger-Procaccia (GP) algorithm [11], which has been demonstrated to work well for long time series from chaotic attractors, works equally well for an ensemble of short transient chaotic time series. In Sec. III, we address the estimation of Lyapunov exponents of chaotic saddles from ensembles of transient chaotic time series. In Sec. IV, we demonstrate that unstable periodic orbits of relatively low period can be detected reliably from ensembles of transient chaotic time series, provided that each individual ensemble is sufficiently large. This result should be useful to experimentalists, because the successful detection of unstable periodic orbits from transient chaotic time series means that (1) the underlying dynamics may exhibit sustained chaotic behavior for nearby parameter values, and (2) many dynamical invariants of the chaotic saddle may be estimated because unstable periodic orbits can be related to the natural measure of the chaotic saddle [12,13]. In Sec. IV, we derive a scaling law for the probability of finding periodic orbits. We have reported briefly in our previous paper [14] on the detection of unstable periodic orbits by utilizing transient chaotic time series from the Hénon map [15]. Besides completeness, the purpose of including Sec. IV is to address detection of unstable periodic orbits embedded in chaotic saddles of more realistic systems. In particular, we utilize a model electrical power system and also the Ikeda-Hammel-Jones-Moloney

(IHJM) map [16] as our examples. Finally, a discussion is presented in Sec. V.

II. COMPUTING THE CORRELATION DIMENSION

All analyses of chaotic time series depend on an appropriate embedding; the time-delay embedding method is one popular method. Given a time series $s(t)$, one forms a sequence of vectors $\mathbf{x}(t) = (s(t), s(t+T), \ldots, s(t+(d-1)T))$, where d is the embedding dimension and T is the delay time. Under mild assumptions about the underlying dynamics, the nature of the measurement function that produces $s(t)$, and the choice of T, it can be shown that various dynamical quantities of the reconstructed set are the same as those of the underlying attractor, provided that d is suitably large [17,18]. In particular, if the correlation dimension of the underlying attractor is D_2, then, for an infinitely long, noiseless time series, the choice of $d \geq D_2$ allows one to determine D_2 from the trajectories in the reconstructed phase space [19], and $d \geq 2D_2 + 1$ suffices to produce a diffeomorphism between the embedded set and the underlying attractor [18].

Almost all works on computing the fractal dimension from chaotic time series address the estimation of the correlation dimension D_2, due to the fundamental observation by Grassberger and Procaccia [11] that D_2 can be evaluated by using the correlation integral $C_N(\epsilon, d)$, which is the probability that a pair of points chosen randomly with respect to the natural measure are separated by a distance less than ϵ on the reconstructed set of phase space of dimension d. For a trajectory of length N, the correlation integral can be approximated by the sum

$$C_N(\epsilon, d) = \frac{2}{N(N-1)} \sum_{j=1}^{N} \sum_{i=j+1}^{N} \Theta(\epsilon - \|\mathbf{x}_i - \mathbf{x}_j\|), \quad (1)$$

where Θ is the Heaviside function [$\Theta(x) = 1$ if $x \geq 0$ and $\Theta(x) = 0$ otherwise], and $\| \cdot \|$ denotes a suitable vector norm, say $\|\mathbf{x}\| = \max\{|\mathbf{x}_i| : 1 \leq i \leq d\}$. Asymptotically, the correlation dimension D_2 is given by [11]

$$D_2 = \lim_{\epsilon \to 0} \lim_{N \to \infty} \frac{\ln C_N(\epsilon, d)}{\ln \epsilon}. \quad (2)$$

For a long time series from a chaotic attractor, the common numerical practice is to extrapolate the slope from a linear fitting of $\ln C_N(\epsilon, d)$ versus $\ln \epsilon$ in an appropriate scaling regime [20] at a set of increasing values of the embedding dimension d. For $d \leq \lfloor D_2 \rfloor$, where $\lfloor D_2 \rfloor$ denotes the largest integer less than or equal to D_2, the slope is equal to d. For $d > \lfloor D_2 \rfloor$, the slope saturates at a constant value which is usually taken to be the estimated value of D_2.

An important question is whether the GP paradigm Eqs. (1) and (2) is applicable to transient time series from chaotic saddles. Here we present a theoretical argument that appears to provide an affirmative answer to this question.

First, we define the natural measure associated with a nonattracting chaotic saddle. Imagine a phase-space region S that contains a nonattracting chaotic saddle. If a large number N_0 of random initial conditions is distributed in S, the corresponding trajectories will leave S eventually as time progresses. They do so by being attracted along the stable manifold, wandering near the chaotic saddle, and then exiting along the unstable manifold. Let $N(n)$ be the number of trajectories that still remain in S at time n. For large n, $N(n)$ decreases exponentially due to the chaotic but nonattracting nature of the saddle [21]:

$$N(n) = N_0 e^{-n/\tau}, \quad (3)$$

where τ is the average lifetime of the trajectories on the chaotic saddle.

Because of the nonattracting nature of the chaotic saddle, the definition of the natural measure is somewhat more complicated than that for a chaotic attractor. Because of the invariance of the natural measure under the dynamics, it is necessary in the definition to compensate for the escape of chaotic trajectories. The standard approach is to choose an ensemble of initial conditions and ask where the resulting trajectories can be at different times. In particular, since trajectories escape from the chaotic saddle along the unstable manifold, at large positive time n, the $N(n)$ trajectory points will be in the vicinity of the unstable manifold. In order for the points to stay near the unstable manifold at time n, initially these points have to be in the vicinity of the stable manifold. At an intermediate time, the points are then concentrated near the chaotic saddle itself. These considerations lead to the formal definitions of the natural measures of the unstable manifold, the stable manifold, and the chaotic saddle [12,22], as follows.

Let C be a small box within S that contains part of the unstable manifold. The natural measure associated with the unstable manifold in C can thus be defined as

$$\mu_u(C) = \lim_{n \to +\infty} \lim_{N_0 \to \infty} \frac{N_u(n, C)}{N(n)}, \quad (4)$$

where $N_u(n, C)$ is the number of the $N(n)$ orbits in C at time n. Similarly, the natural measure of the stable manifold in a box C in S can be defined as

$$\mu_s(C) = \lim_{n \to +\infty} \lim_{N_0 \to \infty} \frac{N_s(n, C)}{N(n)}, \quad (5)$$

where $N_s(n, C)$ is the *number of initial conditions* in C whose trajectories do not leave S before time n. The definitions Eqs. (4) and (5) mean that the natural measures associated with the stable and the unstable manifolds in C are determined by the numbers of trajectory points in C at time zero and time n, respectively. The natural measure of the chaotic saddle, μ, can then be defined by considering $N_m(\rho, n, C)$, the number of trajectory points in C at a time ρn between zero and n:

$$\mu(C) = \lim_{n \to +\infty} \lim_{N_0 \to \infty} \frac{N_m(\rho, n, C)}{N(n)}, \quad (6)$$

where $0 < \rho < 1$, $N_m(0, n, C) = N_s(n, C)$, and $N_m(1, n, C) = N_u(n, C)$. For large N_0 and n, trajectories that remain in S

stay near the chaotic saddle for most of the time between 0 and n, except at the beginning when they are attracted toward the saddle along the stable manifold, and at the end when they are exiting along the unstable manifold. Thus, the measure defined in Eq. (6) is independent of ρ, insofar as $0 < \rho < 1$.

Based on Eq. (6), one can define the following dimension spectrum for nonattracting chaotic saddles [3], in analogy to that of the chaotic attractor [11,23]:

$$D_q = \frac{1}{(q-1)} \lim_{\epsilon \to 0} \frac{\ln I(q,\epsilon)}{\ln \epsilon}, \qquad (7)$$

where q is a continuous index, $I(q,\epsilon) = \sum_{i=1}^{N(\epsilon)} \mu_i^q$, μ_i is the natural measure of the chaotic saddle contained in the ith box, and the sum is over all the $N(\epsilon)$ boxes in a grid of size ϵ needed to cover the whole chaotic saddle. Letting $q = 2$, we obtain

$$D_2 = \lim_{\epsilon \to 0} \frac{\ln \sum_{i=1}^{N(\epsilon)} \mu_i^2}{\ln \epsilon} = \lim_{\epsilon \to 0} \frac{\ln \langle \mu_i \rangle}{\ln \epsilon}, \qquad (8)$$

where $\langle \cdot \rangle$ denotes the phase-space average over the chaotic saddle. For a long, ergodic trajectory on the chaotic saddle, $\langle \mu_i \rangle$ is approximately the probability that the trajectory comes in the ϵ neighborhood of a point $\mathbf{x}_i$ on the chaotic saddle in the ith box, which is given by the correlation integral in Eq. (1). From measurements, we do not have a long, ergodic trajectory on the chaotic saddle. Instead, we can only have M transient chaotic time series, each of length L. Let p_i be the probability that the reconstructed trajectory comes to the neighborhood of $\mathbf{x}_i$. We have

$$p_i \approx \frac{1}{M} \frac{1}{L(L-1)} \sum_{m=1}^{M} \sum_{j=1}^{L} \Theta(\epsilon - \|\mathbf{x}_j^m - \mathbf{x}_i\|), $$

where $\mathbf{x}_j^m$ is the jth trajectory point reconstructed from the mth transient time series. Noting that M is in fact the number N_0 of initial conditions in the definition (6), we have

$$\mu_i \approx \frac{M p_i}{M e^{-L/\tau}} \approx \frac{e^{L/\tau}}{M L(L-1)} \sum_{m=1}^{M} \sum_{j=1}^{L} \Theta(\epsilon - \|\mathbf{x}_j^m - \mathbf{x}_i\|). $$

Averaging over all points $\mathbf{x}_i$ in the reconstructed phase space, we obtain

$$\langle \mu_i \rangle \approx e^{L/\tau} C_{M,L}(\epsilon,d), \qquad (9)$$

where

$$C_{M,L}(\epsilon,d) \equiv \frac{1}{ML(L-1)} \sum_{m=1}^{M} \sum_{i=1}^{L} \sum_{j=1, j \neq i}^{L} \Theta(\epsilon - \|\mathbf{x}_j^m - \mathbf{x}_i^m\|) \qquad (10)$$

is defined to be the correlation integral associated with M observations of transient chaos, each consisting of L points in the reconstructed phase space. We then have

$$D_2 = \lim_{\epsilon \to 0, M \to \infty} \frac{\ln C_{M,L}(\epsilon,d)}{\ln \epsilon}. \qquad (11)$$

Equation (11) indicates that, if one computes the correlation integral as defined in Eq. (10), the GP formulation is valid for transient chaotic time series as well.

To provide numerical support, we consider transient chaotic time series from the Hénon map [15]: $(x,y) \to (a-x^2 +by, x)$ (a and b are parameters) for which the correlation dimension can be obtained both from the GP formulation Eq. (11) and from a straightforward implementation of the box-counting definition (7) by utilizing a long PIM (proper interior maximum) triple trajectory on the chaotic saddle [24]. For $a = 1.5$ and $b = 0.3$, there is a chaotic saddle in the phase-space region $[-2,2] \times [-2,2]$ with lifetime $\tau \approx 30$. The box-counting approach gives $D_2 \approx 1.2$. To apply the GP algorithm, we generate $M = 5000$ transient chaotic time series. To guarantee that each time series reflects, approximately, the natural measure of the chaotic saddle, we disregard both the initial and final phases, and keep only 20 points from the middle of the time series. For a given embedding dimension d, the number of trajectory points corresponding to each time series is then $L < 20$. We choose the delay time to be $T = 1$, normalize each time series to the unit interval, and compute the correlation sum $C_{M,L}(\epsilon,d)$ at 100 values of ϵ for $-30 < \log_2 \epsilon < 0$ using embedding dimensions ranging from $d = 1$ to $d = 8$, as shown in Fig. 1(a). For $d > 3$, the local slopes of the plots appear to converge to a plateau value, as shown in Fig. 1(b). We obtain $D_2 \approx 1.12$, which agrees reasonably well with the value of D_2 obtained from the box-counting algorithm. We note that due to the availability of only short time series the embedding dimension needs to be much larger than the value of D_2 itself to yield the correct plateau value for D_2, in contrast to the case of long time series from chaotic attractors where $d \gtrsim D_2$ usually suffices [19].

III. ESTIMATING LYAPUNOV EXPONENTS

Our approach for obtaining Lyapunov exponents from an ensemble of transient chaotic time series is similar to that in Refs. [25–29]. We apply the same time-delay embedding to each of the transient time series. Linear approximations of the dynamics at each point in the resulting ensemble are constructed using least squares, as described in Ref. [31]. (Care is taken to avoid points in the reconstruction that have no image in the same transient time series.) In this way, we obtain models of the form $\mathbf{y}_j = \mathbf{T}_j \mathbf{x}_j + \mathbf{b}_j$, which approximate the dynamics in a neighborhood of $\mathbf{x}_j$. A QR decomposition of a suitable product of the $\mathbf{T}$'s, as described in Refs. [26–28], can be used to obtain approximations of the Lyapunov exponents.

As a numerical experiment, we generate an ensemble of chaotic transients from the Hénon map for the parameter pairs $(a,b) = (1.46, 0.3)$ and $(a,b) = (1.50, 0.3)$. We generate 21 000 points near the chaotic saddle using 300 random initial conditions in $[-2,2] \times [-2,2]$ for the case $a = 1.46$ and 700 random initial conditions for $a = 1.50$. (The average life-
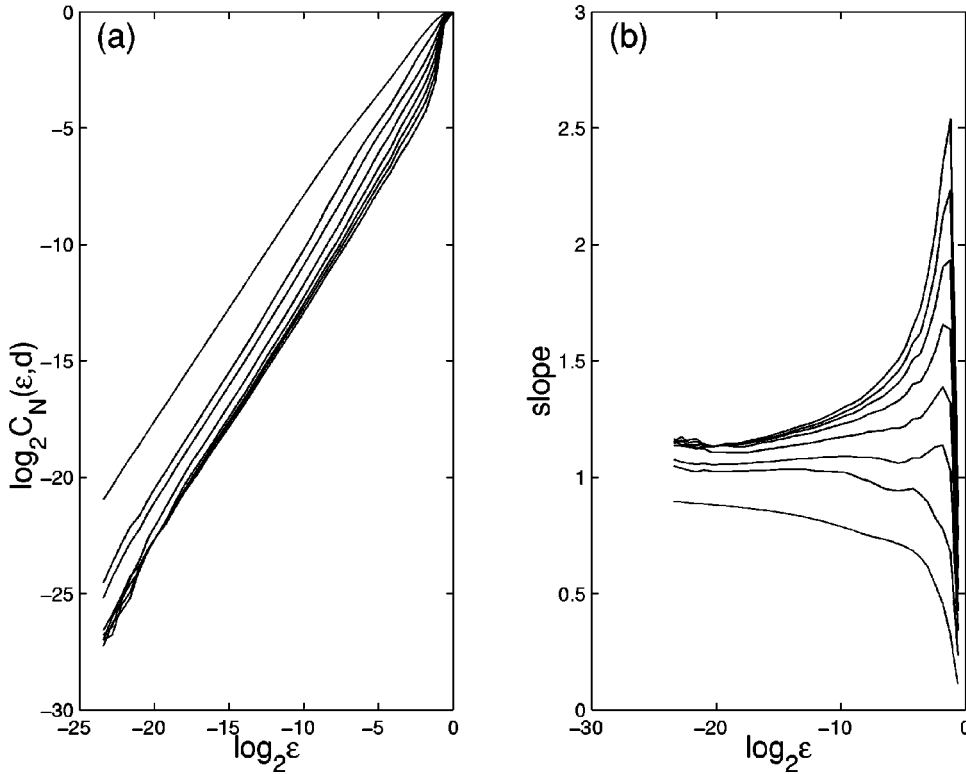
FIG. 1. For the Hénon map, (a) $\log_2 C(\epsilon,d)$ versus $\log_2 \epsilon$, and (b) $\log_2 C(\epsilon,d)/\log_2 \epsilon$ versus $\log_2 \epsilon$ at $a = 1.5, b = 0.3$. The curves with comparatively higher slopes correspond to higher embedding dimensions.

time of the chaotic transients is about 70 iterates for $a = 1.46$ and 30 iterates for $a = 1.50$.) A two-dimensional embedding with a time delay of 1 is constructed from each collection of time series. Local linear maps are computed using least squares for each neighborhood.

In the case $a = 1.46$, each transient time series consists of about 70 iterates. Thus, the ''Lyapunov exponents'' that are computed are actually finite-time approximations, where we consider a suitable product of the 70 or so linear maps associated with points on the individual transient time series. Similarly, when $a = 1.50$, we consider products of 30 or so linear maps. Figure 2(a) shows the distribution of the largest Lyapunov exponent λ_1, computed from the ensembles of time series for $a = 1.46$, and Fig. 2(b) shows the distribution of the values of λ_2. We obtain $\lambda_1 = 0.44 \pm 0.05$ and $\lambda_2 = -1.72 \pm 0.06$ (the second value is the standard deviation of each distribution). Similarly, for $a = 1.50$, we obtain $\lambda_1 = 0.54 \pm 0.06$ and $\lambda_2 = -1.77 \pm 0.08$.

To assess the reliability of these estimates, we compute long PIM triple trajectories of the corresponding chaotic saddles. Then, using the associated Jacobian matrices at each point, we compute finite-time Lyapunov exponents over sections of 70 iterates and 30 iterates, respectively, for $a = 1.46$ and $a = 1.50$. Figure 3 shows the resulting distributions, which are centered around $\lambda_1 = 0.44$ and $\lambda_2 = -1.64$ ($a = 1.46$), and $\lambda_1 = 0.54$ and $\lambda_2 = -1.72$ ($a = 1.50$). (The standard deviations are small.) This numerical experiment suggests that the Lyapunov exponents from low dimensional chaotic saddles can be computed with reasonable accuracy, provided that sufficiently many observations are available and the noise level is low. Specifically, for noise below $\epsilon = 10^{-1}$ (about 2.5% of the transient chaotic signal) in the Hénon map, the estimates of the Lyapunov exponent are still

relatively accurate, particularly for the positive exponent, as shown in Figs. 4(a) and 4(b) for transient chaos at $a = 1.46$ and $a = 1.50$, respectively. In the figures, the dashed lines indicate the correct values of the corresponding positive and negative exponents. We note that the difficulty in obtaining good estimates for the negative Lyapunov exponents from time series is a common problem even for sustained chaos [27], because of the issue of accurately determining the *full* Jacobian matrices [30].
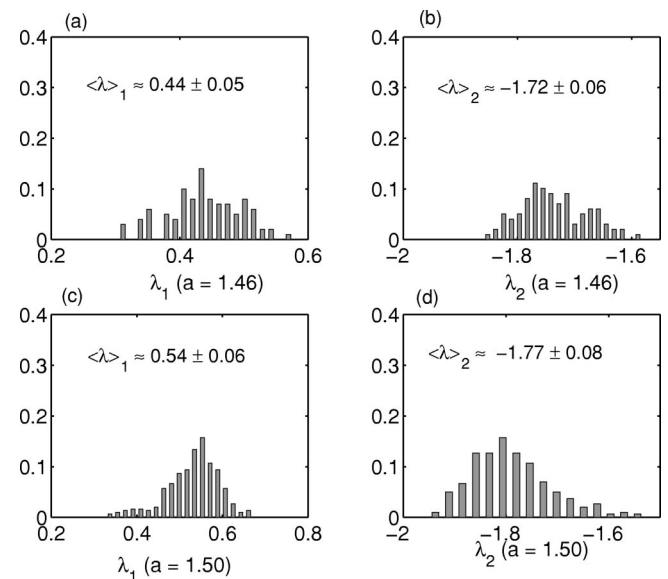

FIG. 2. (a)–(d) The distributions of Lyapunov exponents of the Hénon map for chaotic transients at the two parameter values of $a = 1.46$ and $a = 1.50$, respectively.
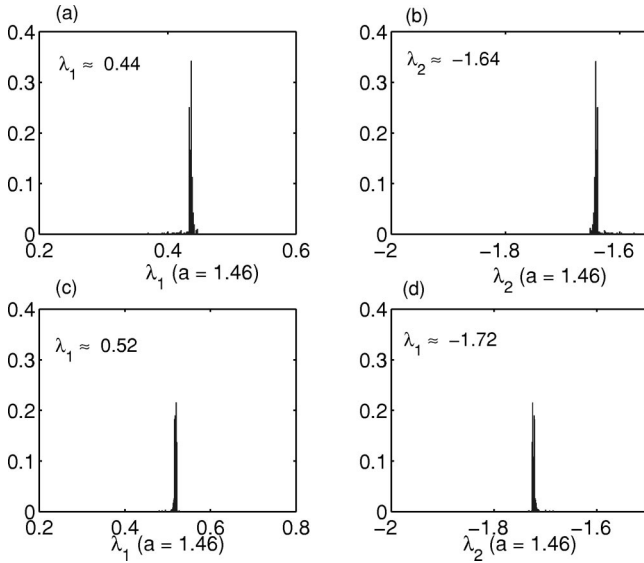
FIG. 3. (a)–(d) The distributions of finite-time Lyapunov exponents of the Hénon map from the PIM triple trajectory at the two parameter values of $a = 1.46$ and $a = 1.50$, respectively.

IV. DETECTING UNSTABLE PERIODIC ORBITS

Lathrop and Kostelich (LK) [32] describe a simple algorithm to identify unstable periodic orbits from long time series from chaotic attractors, which is based on locating sets of recurrent points in the reconstructed attractor [33]. Given a positive ϵ, one follows successive images of a starting a point $\mathbf{x}(t)$ to determine whether a value $m > 0$ exists such that $\|\mathbf{x}(t+m) - \mathbf{x}(t)\| < \epsilon$. If such an m exists, then $\mathbf{x}(t)$ is an (m, ϵ) *recurrent point*, and m is the recurrence time. A recurrent point needs not be periodic, but points that lie sufficiently close to periodic orbits are recurrent. Histograms of recurrence times from embedded attractors can then be constructed and examined for values of m that occur frequently.
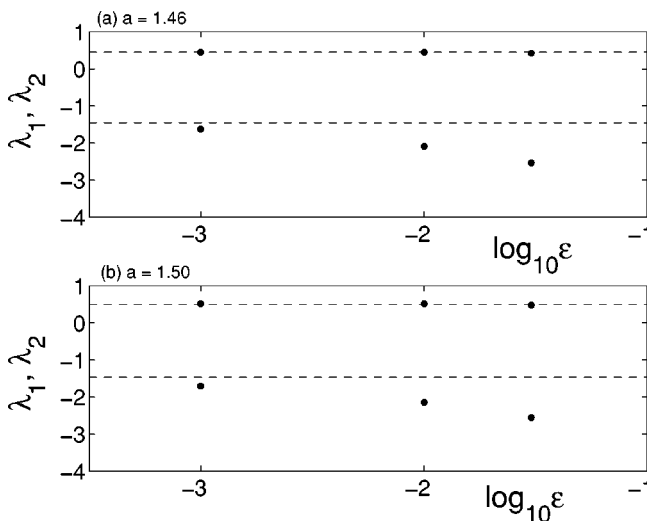

FIG. 4. For transient chaos in the Hénon map, effect of noise on computation of Lyapunov exponents: (a) $a = 1.46$ and (b) $a = 1.50$. The dashed lines indicate the values of the two exponents in the absence of noise.
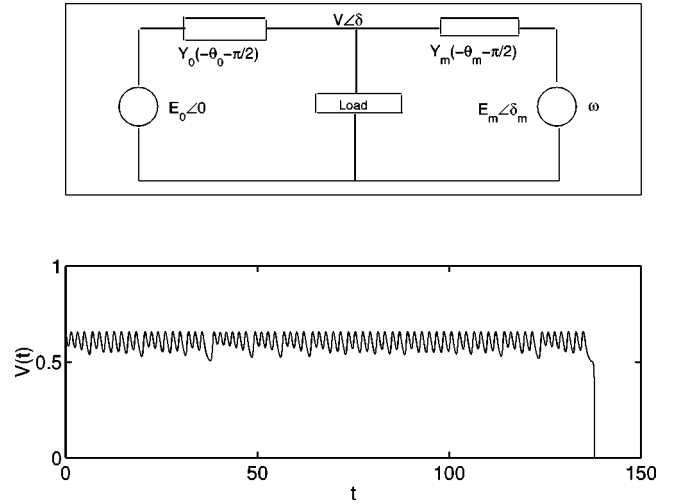

FIG. 5. For the electrical power system (a) the model network, and (b) a chaotic transient.

For long chaotic time series, unstable periodic orbits can be traced by following trajectories starting from the corresponding (m, ϵ) recurrent points.

In Ref. [14], the LK algorithm is adapted to detecting unstable periodic orbits from an ensemble of transient chaotic time series. The idea is essentially the same as that in the original formulation of the LK algorithm [32], i.e., to accumulate a histogram of recurrence times from all time series in the ensemble. As each individual time series is short, we expect to be able to detect at least periodic orbits of short periods (the issue of long periods is addressed later in this section). It is not necessary to attempt to concatenate many short time series into a single long one, an approach that is usually problematic [5].

We have implemented and tested the LK algorithm for detecting unstable periodic orbits from various models of chaotic systems. Here we report numerical results with transient time series of an electrical power system network model at voltage collapse [34,35]. The electrical power system is modeled by the network shown in Fig. 5(a). The model consists of two generators (with voltages E_0 and E_m) and a load (consisting of an induction motor and a PQ load in parallel). There are four dynamical variables: (1) δ_m, the generator phase angle, which is closely related to the mechanical angle of the rotor; (2) ω, the angular speed of the rotor; (3) δ, the load voltage phase angle; and (4) V, the magnitude of the voltage provided to the load. The system is described by the four autonomous ordinary differential equations [34]

$$\dot{\delta}_m = \omega,$$

$$M\dot{\omega} = -d_m \omega + P_m - E_m V Y_m \sin(\delta_m - \delta),$$

$$K_{qw}\dot{\delta} = -K_{qv2}V^2 - K_{qv}V + Q(\delta_m, \delta, V) - Q_0 - Q_1,$$
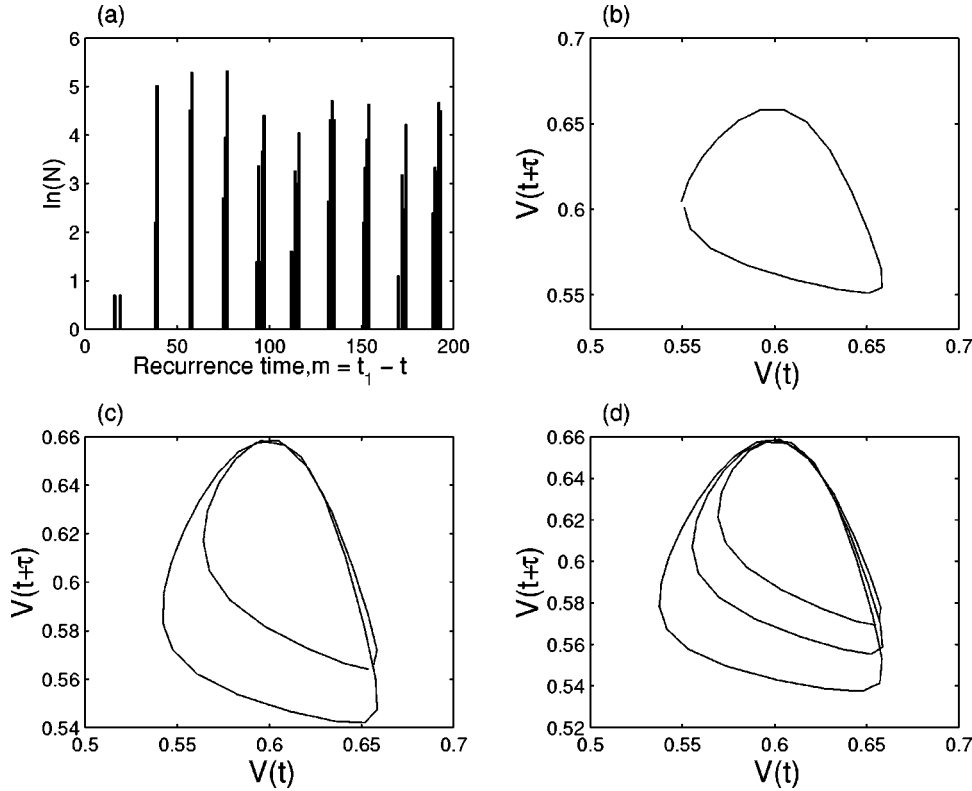
FIG. 6. For the electrical power system, (a) a histogram of recurrence time, trajectories near (b) period-1, (c) period-2, and (d) period-3 saddle.

$$TK_{qw}K_{pv}\dot{V} = K_{pw}K_{qv2}V^2 + (K_{pw}K_{qv} - K_{qw}K_{pv})V$$
$$+ K_{qw}[P(\delta_m,\delta,V) - P_0 - P_1]$$
$$- K_{pw}[Q(\delta_m,\delta,V) - Q_0 - Q_1]. \quad (12)$$

The real and reactive powers supplied to the load by the network are

$$P(\delta_m,\delta,V) = -E_0VY_0 \sin\delta + E_mVY_m \sin(\delta_m - \delta),$$

$$Q(\delta_m,\delta,V) = E_0VY_0 \cos\delta + E_mVY_m \cos(\delta_m - \delta)$$
$$- (Y_0 + Y_m)V^2.$$

In our numerical simulation, the load, the network, and the generator parameter values are chosen to be [34,35] $K_{pw} = 0.4$, $K_{pv} = 0.3$, $K_{qw} = -0.03$, $K_{qv} = -2.8$, $K_{qv2} = 2.1$, $T = 8.5$, $P_0 = 0.6$, $Q_0 = 0.3$, $P_1 = 0.0$, $Y_0 = 3.33$, $Y_m = 5.0$, $P_m = 1.0$, $d_m = 0.05$, $M = 0.014\,64$, $E_m = 1.05$, $\theta_0 = 0$, and $\theta_m = 0$.

There is a period-doubling cascade to chaos, and a crisis occurs at $Q_{1c} \approx 2.560$, after which the chaotic attractor is converted into a chaotic saddle. Figure 5(b) shows a transient voltage signal after the crisis. These time series are assumed to be the only available data about the system. We then collect a number of such transient time series, construct the corresponding time-delay embeddings, and apply the LK algorithm to each. We take ϵ to be 2% of the root-mean-square value of the time series. Figure 6(a) shows the histogram of the recurrence times obtained by combining the statistics from the entire ensemble of time series. Figures 6(b)–6(d) show, respectively, trajectories near period-1, period-2,

and period-3 orbits [36]. These sample orbits belong to the set of recurrent points comprising the corresponding cluster of peaks in the histogram. In general, the LK algorithm can identify many periodic orbits of low period.

In an experimental setting, time series are usually contaminated by dynamical and/or observational noise. Noise reduces the volume of every recurrent region in the phase space and hence reduces the number of observed recurrent points. A previous analysis [14] shows that the number of observed recurrent points decreases linearly with increasing noise level. Nevertheless, numerical experiments suggest that the LK algorithm can be used to identify potential saddle periodic orbits even if the noise level is as large as 1% of the root-mean-square value of the signal.

We now consider the probability of detecting periodic orbits from transient chaotic time series [37]. This consideration is particularly relevant for transient chaos, because trajectories on a chaotic saddle have an average lifetime τ of staying near the saddle and hence it is unlikely that a typical trajectory contains periodic orbits of period larger than approximately τ. In our previous work [14], we have shown that the probability of detecting periodic orbits decreases exponentially with increasing period. This result is an intrinsic dynamical property of the underlying chaotic saddle. Hence, it is unlikely to observe periodic orbits of high period even if the number of measurements is increased or the noise level is reduced.

The probability $\Phi(p)$ that a typical trajectory is found in an ϵ neighborhood of *any* period-p orbit is [14]

$$\Phi(p) \sim e^{-\lambda_1 D_1 p}N(p) \sim e^{(-\lambda_1 D_1 + h_T)p} = e^{-\gamma p}, \quad (13)$$

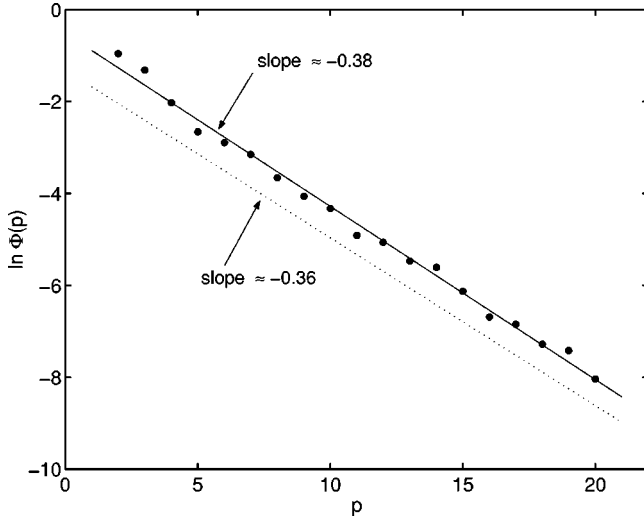where γ is the exponential scaling exponent, h_T is the topo-

FIG. 7. For the map (15) at $C_1 = 0.4$, $C_2 = 0.9$, $C_3 = 6$, and $R = 1.1$, $\ln \Phi(p)$ versus p. The dotted line indicates the theoretically predicted slope of $\ln \Phi(p)$ versus p.

logical entropy, $N(p)$ is the number of periodic orbits of period p, λ_1 is the largest Lyapunov exponent, and D_1 is the information dimension of the chaotic saddle. The Kaplan-Yorke formula [22] relates D_1 to the Lyapunov exponents and the mean lifetime τ of chaotic transients as $D_1 = (\lambda_1 - 1/\tau)(1/\lambda_1 + 1/|\lambda_2|)$. This result and Eq. (13) yield the scaling exponent

$$\gamma = \lambda_1 - h_T + \frac{\lambda_1^2}{|\lambda_2|} - \frac{1}{\tau}\left(1 + \frac{\lambda_1}{|\lambda_2|}\right). \quad (14)$$

The scaling relation in Eq. (13) and the analysis leading to the scaling exponent in Eq. (14) are applicable to chaotic saddles of two-dimensional invertible maps and three-dimensional flows. Note that for chaotic attractors ($\tau \to \infty$) we have $\gamma \approx \lambda_1 - h_T + \lambda_1^2/|\lambda_2|$.

Here we test Eqs. (13) and (14) numerically using chaotic saddles in the IHJM map [16]

$$x_{n+1} = R + C_2(x_n \cos \tau - y_n \sin \tau),$$

$$y_{n+1} = C_2(x_n \sin \tau + y_n \cos \tau), \quad (15)$$

where $\tau = C_1 - C_3/(1 + x_n^2 + y_n^2)$ is the phase variable, and C_1, C_2, C_3, and R are parameters. The unstable periodic orbits are computed utilizing the method in Ref. [38]. There is a chaotic saddle for the following set of parameter values: $C_1 = 0.4$, $C_2 = 0.9$, $C_3 = 6$, and $R = 1.1$, which is contained in the phase-space region $[-0.5, 2.0] \times [-2.5, 1]$. We choose 10^6 random initial conditions in this region to obtain 10^6 transient time series, each of length of about 28. For each period p, we compute the frequency with which orbits on the time series fall into a neighborhood [39] of a saddle periodic orbit of period p. The results are accumulated to determine

$\Phi(p)$. Figure 7 shows a plot of $\ln \Phi(p)$ versus p, which suggests an exponential decay with increasing p, where the decay exponent γ is given by the slope of the plot. To compute the theoretical scaling exponents in Eq. (14), it is necessary to compute the Lyapunov exponents, the topological entropy, and the lifetime of the chaotic saddles. The following numerical algorithms are employed: (1) the PIM triple algorithm [24,40] for a long continuous trajectory on the saddle (the Jacobian matrix is evaluated at each point on the trajectory and the resulting collection is used to compute the Lyapunov exponents of the chaotic saddle); (2) the algorithm in Ref. [41] for computing the topological entropy of the chaotic saddle; and (3) the sprinkler method [22] for estimating the lifetime τ. For the IHJM map with the stated parameter values, these computations yield $\lambda_1 = 0.56$, $\lambda_2 = -0.77$, $h_T = 0.54$, and $\tau = 28$. The slope of the fitted straight line in Fig. 7 is 0.384 ± 0.015. The theoretical scaling exponent is $\gamma \approx 0.365$, as indicated by the dashed straight line in Fig. 7. We see that the exponent extrapolated from the direct numerical simulation of $\Phi(p)$ agrees reasonably well with the predicted one in Eq. (14), which supports the argument that the probability of finding unstable periodic orbits in experimentally measured transient time series decreases exponentially with increasing period.

V. DISCUSSION

In this work, we demonstrate that the GP algorithm is generally applicable for estimating the correlation dimension of the chaotic saddle from an ensemble of transient chaotic time series. We present a numerical procedure with the example of the Hénon map to find the rates of separation of neighboring phase-space states constructed from each transient time series in an ensemble to extract Lyapunov exponents. We also show that unstable periodic orbits of low period can be detected reliably from an ensemble of transient chaotic time series by using the LK algorithm. Our numerical analysis indicates that the LK algorithm is powerful for extracting unstable periodic orbits at low noise level. We further give a theoretical justification for the difficulty of detecting periodic orbits of high period from transient chaos. The theoretical scaling law is verified by numerical examples. Since the probability of detecting these orbits is exponentially small, as a matter of practicality it is perhaps worthless to obtain long time series or to improve the technique for detecting periodic orbits from transient chaos. We remark that, although there has been a tremendous amount of work on analyzing time series from chaotic attractors, the analysis of transient chaotic time series remains a far less explored area.

[1] C. Grebogi, E. Ott, and J.A. Yorke, Physica D **7**, 181 (1983).

[2] H. Kantz and P. Grassberger, Physica D **17**, 75 (1985).

[3] T. Tél, in *Directions in Chaos*, edited by Bai-lin Hao (World Scientific, Singapore, 1990), Vol. 3; in *STATPHYS 19*, edited by Bai-lin Hao (World Scientific, Singapore, 1996).

[4] Analyzing chaotic time series is such a rich field that even a partial list of the relevant papers is impossible here. See, for example, H. Kantz and T. Schreiber, *Nonlinear Time Series Analysis* (Cambridge University Press, Cambridge, 1997), and references therein.

[5] We are aware of only the following paper on analyzing *transient* chaotic time series, which focuses on the reconstruction of the vector space by using embedding: I.M. Jánosi and T. Tél, Phys. Rev. E **49**, 2756 (1994).

[6] Chaos **3**(4) (1993), focus issue.

[7] S.W. McDonald, C. Grebogi, E. Ott, and J.A. Yorke, Physica D **17**, 125 (1985).

[8] See, for example, C. Jung, T. Tél, and E. Ziemniak, Chaos **3**, 555 (1993); Á. Péntek, Z. Toroczkai, T. Tél, C. Grebogi, and J.A. Yorke, Phys. Rev. E **51**, 4076 (1995); Z. Neufeld and T. Tél, *ibid.* **57**, 2832 (1998).

[9] Z. Toroczkai, G. Károlyi, Á. Pétek, T. Tél, and C. Grebogi, Phys. Rev. Lett. **80**, 500 (1998), and references therein.

[10] See, for example, A. Katok, Publ. Math. IHES **51**, 377 (1980); T. Morita, H. Hata, H. Mori, T. Horita, and K. Tomita, Prog. Theor. Phys. **78**, 511 (1987); G.H. Gunaratne and I. Procaccia, Phys. Rev. Lett. **59**, 1377 (1987); D. Auerbach, P. Cvitanović, J.-P. Eckmann, G.H. Gunaratne, and I. Procaccia, *ibid.* **58**, 2387 (1987); P. Cvitanović, Chaos **2**, 1, 61, and 85 (1992), focus issue on periodic orbit theory.

[11] P. Grassberger and I. Procaccia, Phys. Rev. Lett. **50**, 346 (1983); Physica D **9**, 189 (1983).

[12] C. Grebogi, E. Ott, and J.A. Yorke, Phys. Rev. A **37**, 1711 (1988).

[13] M. Dhamala and Y.-C. Lai, Phys. Rev. E **60**, 6176 (1999).

[14] M. Dhamala, Y.-C. Lai, and E.J. Kostelich, Phys. Rev. E **61**, 6485 (2000).

[15] M. Hénon, Commun. Math. Phys. **50**, 69 (1976).

[16] K. Ikeda, Opt. Commun. **30**, 257 (1979); S.M. Hammel, C.K.R.T. Jones, and J. Moloney, J. Opt. Soc. Am. B **2**, 552 (1985).

[17] F. Takens, in *Dynamical Systems and Turbulence*, edited by D. Rand and L.S. Young, Vol. 898 of *Lecture Notes in Mathematics* (Springer-Verlag, Berlin, 1981), p. 366; N.H. Packard, J.P. Crutchfield, J.D. Farmer, and R.S. Shaw, Phys. Rev. Lett. **45**, 712 (1980).

[18] T. Sauer, J.A. Yorke, and M. Casdagli, J. Stat. Phys. **65**, 579 (1991).

[19] M. Ding, C. Grebogi, E. Ott, T. Sauer, and J.A. Yorke, Phys. Rev. Lett. **70**, 3872 (1993).

[20] Y.-C. Lai and D. Lerner, Physica D **115**, 1 (1998).

[21] Exponential decay of the number of trajectories near the chaotic saddle is characteristic of transient chaos in dissipative dynamical systems. In particular, say we sprinkle a large number N_0 of initial conditions in a phase-space region containing the chaotic saddle and compute $N(t)$, the number of trajectories still remaining in the region at time t. Then one typically finds that $N(t)$ decays exponentially with time [1–3]. For simple one-dimensional maps such as the piecewise linear one on the unit interval, $x_{n+1} = 2\eta x_n$ if $0 \leq x_n < 1/2$ and $x_{n+1} = 2\eta(x_n - 1) + 1$ if $1/2 < x \leq 1$, where $\eta \gtrsim 1$, it can be argued easily that there is a chaotic saddle in the unit interval with the exponential decay law: $N(t) \sim \exp(-n/\tau)$, where $\tau = \{\ln[\eta/(\eta - 1)]\}^{-1}$ is the average lifetime of trajectories on the chaotic saddle.

[22] G.-H. Hsu, E. Ott, and C. Grebogi, Phys. Lett. A **127**, 199 (1988).

[23] J.D. Farmer, E. Ott, and J.A. Yorke, Physica D **7**, 153 (1983).

[24] The PIM triple method is for efficiently computing long trajectories on nonattracting chaotic saddles in two-dimensional maps or in three-dimensional flows [H.E. Nusse and J.A. Yorke, Physica D **36**, 137 (1989)]. A PIM triple is three points (a,c,b) in a straight line segment such that the interior point c (i.e., c is between a and b) has an escape time larger than those of both a and b so that the triple (a,c,b) has a proper interior maximum. Briefly, the steps of the PIM triple procedure are as follows. (1) Choose a line segment L_0 in a region that contains the chaotic saddle. Distribute uniformly a number of points on the line segment and calculate the escape time for each point. Choose any PIM triple (a,c,b) from the points. (2) Use the PIM triple as the new line segment and repeat step 1 until the length of the PIM triple so obtained is less than, say, 10^{-9} (denoted by I_0). Write $I_0 = R(L_0)$, that is, I_0 is the refined L_0. (3) Iterate the end points of I_0 forward. The two images are end points of a new segment denoted by L_1. Repeat step 2, if necessary, to ensure that the length of L_1 is less than 10^{-9}. (4) Repeat step 3 to find a sequence of PIM triple intervals, which represents a continuous trajectory on the chaotic saddle.

[25] V.I. Oseledec, Tr. Mosk. Mat. Obsc. **19**, 17 (1968).

[26] J.-P. Eckmann and D. Ruelle, Rev. Mod. Phys. **57**, 617 (1985).

[27] J.-P. Eckmann, S.O. Kamphorst, D. Ruelle, and S. Ciliberto, Phys. Rev. A **34**, 4971 (1986).

[28] A. Wolf, J.B. Swift, H.L. Swinney, and J.A. Vastano, Physica D **16**, 285 (1985).

[29] M. Sano and Y. Sawada, Phys. Rev. Lett. **55**, 1082 (1985).

[30] T.D. Sauer, J.A. Tempkin, and J.A. Yorke, Phys. Rev. Lett. **81**, 4341 (1998); T.D. Sauer and J.A. Yorke, *ibid.* **83**, 1331 (1999).

[31] E.J. Kostelich and J.A. Yorke, Physica D **41**, 183 (1990).

[32] D.P. Lathrop and E.J. Kostelich, Phys. Rev. A **40**, 4028 (1989).

[33] Detection of unstable periodic orbits embedded in chaotic attractors has been an active area of investigation. For additional work besides Ref. [32], see, for example, G.B. Mindlin, X.-J. Hou, H.G. Solari, R. Gilmore, and N.B. Tufillaro, Phys. Rev. Lett. **64**, 2350 (1990); K. Pawelzik and H.G. Schuster, Phys. Rev. A **43**, 1808 (1991); D. Pierson and F. Moss, Phys. Rev. Lett. **75**, 2124 (1995); R. Badii *et al.*, Rev. Mod. Phys. **66**, 1389 (1994); D.J. Christini and J.J. Collins, Phys. Rev. Lett. **75**, 2782 (1995); X. Pei and F. Moss, Nature (London) **379**, 619 (1996); P. So, E. Ott, S.J. Schiff, D.T. Kaplan, T. Sauer, and C. Grebogi, Phys. Rev. Lett. **76**, 4705 (1996); P. Schmelcher and F.K. Diakonos, *ibid.* **78**, 4733 (1997); S. Allie and A. Mees, Phys. Rev. E **56**, 346 (1997); S.M. Zoldi and H.S. Greenside, *ibid.* **57**, R2511 (1998).

[34] I. Dobson and H.-D. Chiang, Syst. Control Lett. **13**, 253 (1989); H. Wang, E.H. Abed, and A.M.A. Hamdan (unpublished); H. Wang and E.H. Abed (unpublished).

[35] M. Dhamala and Y.-C. Lai, Phys. Rev. E **59**, 1646 (1999).

[36] The orbit shown in Fig. 6(b) is the orbit of shortest period that is identified using the LK algorithm, and the term ''period-1'' is a simple normalization; the period of the corresponding saddle orbit in the system (12) is not $T=1$ for the parameters given there. The periods of the orbits in Figs. 6(c) and 6(d) are almost exactly two and three times larger, respectively, so we refer to them as ''period 2'' and ''period 3.''

[37] The corresponding problem for chaotic attractors was discussed by X. Pei, K. Dolan, F. Moss, and Y.-C. Lai, Chaos **8**, 853 (1998). The definition of the probability studied in that paper was, however, slightly different from the one considered in the present paper.

[38] R.L. Davidchack and Y.-C. Lai, Phys. Rev. E **60**, 6172 (1999).

[39] Here the ''neighborhood'' refers, roughly, to a small region surrounding the periodic orbit in which the linearized dynamics holds. The size of the neighborhood thus depends on the eigenvalues of the periodic orbit and decreases exponentially as the period is increased. For unstable periodic orbits of low period treated in this paper, we find that a good linear neighborhood has a size on the order of 10^{-3}.

[40] J. Jacobs, E. Ott, and C. Grebogi, Physica D **108**, 1 (1997).

[41] Q. Chen, E. Ott, and L.P. Hurd, Phys. Lett. A **156**, 48 (1991). The algorithm uses the fact that the metric entropy nearly equals the topological entropy in typical cases. One first specifies the region of interest and takes a line segment AB that straddles the stable manifold. Then AB is subdivided with many points and the lifetimes of trajectories are calculated under the inverse dynamics (if the system is invertible), where the lifetime is the time within which a trajectory remains in the region. Then in the lifetime plots one counts the number of subintervals Σ_n whose lifetime is greater than or equal to n. Since Σ_n scales with n as $\Sigma_n \sim e^{h_T n}$, the slope of such a plot gives an estimate of the topological entropy h_T of the chaotic saddle. Here we note that the topological entropy for the inverse dynamics is the same as that for the direct dynamics; see R.C. Adler, A.C. Konheim, and M.H. McAndrew, Trans. Am. Math. Soc. **114**, 309 (1965).